Annals of Biomedical Engineering, Vol. 46, No. 7, July 2018 *(© 2018)* pp. 1047–1065
https://doi.org/10.1007/s10439-018-2020-z

A Semi-passive Planar Manipulandum for Upper-Extremity Rehabilitation

CHIH-KANG CHANG,[1] EDWARD P. WASHABAUGH,[1,2] ANDREW GWOZDZIOWSKI,[1] C. DAVID REMY,[3,4] and CHANDRAMOULI KRISHNAN[1,2,4]

[1]Neuromuscular and Rehabilitation Robotics Laboratory (NeuRRo Lab), Department of Physical Medicine and Rehabilitation, University of Michigan, Ann Arbor, MI, USA; [2]Department of Biomedical Engineering, University of Michigan, Ann Arbor, MI, USA; [3]RAM Lab, Department of Mechanical Engineering, University of Michigan, Ann Arbor, MI, USA; and [4]Michigan Robotics, College of Engineering, University of Michigan, Ann Arbor, MI, USA

(Received 27 December 2017; accepted 29 March 2018; published online 6 April 2018)

Associate Editor Xiaoxiang Zheng oversaw the review of this article.

Abstract—Robotic rehabilitation is a promising approach to treat individuals with neurological or orthopedic disorders. However, despite significant advancements in the field of rehabilitation robotics, this technology has found limited traction in clinical practice. A key reason for this issue is that most robots are expensive, bulky, and not scalable for in-home rehabilitation. Here, we introduce a semi-passive rehabilitation robot (SepaRRo) that uses controllable passive actuators (i.e., brakes) to provide controllable resistances at the end-effector over a large workspace in a manner that is cost-effective and safe for in-home use. We also validated the device through theoretical analyses, hardware experiments, and human subject experiments. We found that by including kinematic redundancies in the robot's linkages, the device was able to provide controllable resistances to purely resist the movement of the end-effector, or to gently steer (i.e., perturb) its motion away from the intended path. When testing these capabilities on human subjects, we found that many of the upper-extremity muscles could be selectively targeted based on the forcefield prescribed to the user. These results indicate that SepaRRo could serve as a low-cost therapeutic tool for upper-extremity rehabilitation; however, further testing is required to evaluate its therapeutic benefits in patient population.

Keywords—Kinematics, Design, Simulation, Planar, Two-dimensional, Reaching, Feedback.

ABBREVIATIONS

SepaRRo	Semi-passive rehabilitation robot
GUI	Graphical user interface
NNLS	Non-negative least squares
PWM	Pulse width modulation
EMG	Electromyography
MVC	Maximum voluntary contraction
ANOVA	Analysis of variance
PMC	Pectoralis major (clavicular)
PMS	Pectoralis major (sternal)
LD	Latissimus dorsi
Delt	Deltoid
BB	Biceps brachii
BR	Brachioradialis
TB	Triceps brachii
WF	Wrist flexors
WE	Wrist extensors

INTRODUCTION

The fields of robotics and physical therapy are quickly converging. As our population ages, the number of individuals needing rehabilitation is expected to increase worldwide and the number of interventions to address motor disability must grow accordingly.[33]

Appropriately designed rehabilitation devices can assist in meeting this heightened demand for care by augmenting, partially automating, and diversifying the interventions that can be delivered by a therapist.[1,20,30] end As a consequence, there has been a rise in demand

Address correspondence to Chandramouli Krishnan, Neuromuscular and Rehabilitation Robotics Laboratory (NeuRRo Lab), Department of Physical Medicine and Rehabilitation, University of Michigan, Ann Arbor, MI, USA. Electronic mail: mouli@umich.edu

Chih-Kang Chang and Edward P. Washabaugh have equally contributed to this work.

0090-6964/18/0700-1047/0 © 2018 Biomedical Engineering Society

for robotic solutions that can augment, automate, and personalize patient treatment.[34] These devices deliver repetitive, task-specific treatment to the patient, while simultaneously monitoring their progress.[9] Furthermore, robotic solutions can relieve the therapist from physical training effort and quantify the level of motor recovery.[13] It is particularly useful if such robotic solutions can be used at home, as recent studies indicate that take-home robots can improve the effects of rehabilitation by enabling a greater volume of therapeutic exercise[22,43,44,46]—which is perhaps the most important determinant to a patient's recovery.

With these goals in mind, a number of upper-extremity rehabilitation robotic devices have been developed in the past two decades.[20,29,30,36] Many of these robots are built with active actuators (i.e., motors) and are primarily used as assistive devices, where the robot performs the movement for the patient or forces them along a predefined path. While assistive therapy is reasonable for a patient who is early in his/her rehabilitation process, it may not be the best approach for someone who has already regained some of their lost functions, as assistance may fail to engage them in training.[31,37,47] For this reason, some motorized robots have been adapted to incorporate resistive brakes or challenge-based control algorithms to increase the difficulty of training or resist the user's movements.[3,4,6,14,21,30] However, because these robotic devices use active actuators, they are typically expensive, bulky, and can even be potentially unsafe if not programmed correctly, which prevents them from being used in the comfort of a patients home.

Thus, patients often rely on low-cost passive devices (e.g., elastic bands, weights, *etc.*), which can be obtained at a fraction of the cost, to address deficits in muscle strength and movement control during in-home rehabilitation. While devices such as elastic bands and weights are simple and safe to use in a home environment, they are not controllable and cannot be scaled efficiently for adequate progression during rehabilitation. Hence, there is a large need for cost-effective robotic therapy solutions that can be used outside the clinic.

Until active robotic systems become cheaper and more lightweight, for example through the development of new soft robotic technology, semi-passive rehabilitation robots may be capable of filling the gap between active rehabilitation robots and traditional passive exercise equipment. Unlike active robots, semi-passive robots do not have big motors, but deliver therapy by relying solely on controllable dissipative elements such as adjustable brakes, clutches, or dampers. There is one drawback: by removing motors, semi-passive robots lose the ability to add mechanical energy to the user, and therefore, cannot provide the typical assistance to motion (Note: for the purposes of this paper we are not considering passive spring-based *assistive* devices, such as the Armeo Spring). However, resistive training has been shown to have clinical benefits,[31,47] and with careful design, semi-passive robots can be made to approximate the functions of active robots by providing steering forces or even rendering virtual objects similar to passive haptic interfaces.[5,15,16] There are additional benefits to this approach: because mechanical energy is not added to the user, these devices are inherently safe. Furthermore, dissipative elements are typically less expensive, lighter, and more compact than the active actuators used in similar applications.[8]

Thus, the inherent safety, low-cost, lightweight, and more compact features of semi-passive rehabilitation robots can potentially make them portable for in-home use. However, many existing devices that fall within this semi-passive class for rehabilitation—although clever in design and implementation—may fail to capitalize on these perceived benefits. Many of these devices are aimed to provide a 3-dimensional reaching workspace, but this requires them to have bulky systems to counterbalance the device weight.[10,39] Whereas others have a configuration that does not allow for extensive steering forces,[19,24] or are incapable of providing large resistances.[35]

In this paper, we present a prototype of a complete dissipative device: the semi-passive rehabilitation robot (SepaRRo), which is specifically targeted towards therapy for the upper-extremity. The robot was especially designed to provide large controllable resistance against a patient's motion as well as gently steer the movements of the user. The direction and magnitude of the resistive force can be continually adjusted based on a patient's ability level and rehabilitation needs through open-loop control with an Arduino UNO microprocessor. It also enables a real-time response in reaction to a patient's motion; thus, allowing for path-dependent resistances, deliberate disturbances, and supportive control. Further, the robot is designed specifically with cost, weight, portability, and safety in mind. Our ultimate goal is that SepaRRo can be used easily in a patients home and without the need for supervision.

SepaRRo consists of a handle that is attached to the end-effector of a mechanical linkage (Figs. 1a and 1b). The user can grab the handle or be strapped to it if they have limited hand function. The linkage enables motion of the end-effector in a 2D plane without constraining the reachable workspace of the user's arm. The plane can be tilted at a number of inclinations to enable functional reaching movements in both gravity-eliminated and gravity-resisted positions (Fig. 1c), which are critical for robots that incorporate resistive strategies.[30] Scalable resistance to motion is

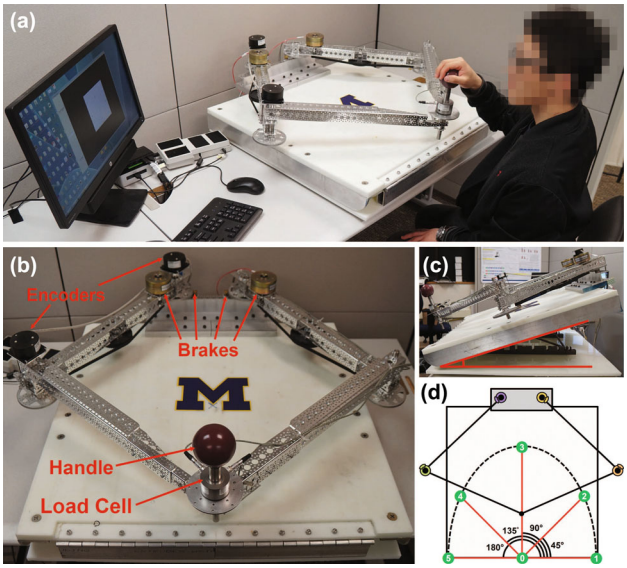

FIGURE 1. Overview of the semi-passive rehabilitation robot (SepaRRo). (a) A user interacts with the end-effector (i.e., handle) of the device while receiving feedback from a monitor. (b) The robot consists of two two-joint planar manipulators connected at the end-effector. Four brakes provide resistance at the joints. Encoders measure the joint angles and allow for the calculation of the end-effector position and velocity. A load cell is connected to the end-effector for force validation of the device. (c) A hinge at the front of the table allows the robot to be tilted for training in gravity-resisted positions. (d) Schematic depicting the feedback provided through the graphical user interface (GUI) of the robot. The image displays the position of the end-effector in real-time along with the designated reaching paths that were used in the hardware and human subject experiments.

provided by magnetic particle brakes in the linkage, while encoders and force sensors record the motion and effort put forth by the user. A graphical user interface (GUI) shows the desired motion, allows programming the resistance, and displays the forces experienced by the user.

This paper focuses specifically on the hardware, working principle, and controller that is used in SepaRRo. We discuss the design challenges for such a semi-passive robot, including the need for a kinematic configuration (i.e., layout and number of linkages) with carefully selected redundancies (Fig. 2). This redundant design is necessary to achieve a broad range of resistive forces at the end-effector over the entire reachable workspace of the patient. In the absence of active actuators, the robot is not completely controllable; therefore, unique controls are implemented in order to apply the intended resistance to a patients movement. We carefully designed, implemented, and tested a prototype that applied this theoretical background in order to establish its potential use for rehabilitation applications. Furthermore, we applied this prototype in an experiment on healthy human subjects to demonstrate examples of variable intensity resistance with this robotic device.

MATERIALS AND METHODS

In the following sections, we first derive the mathematical theory of the working principle of SepaRRo ("Working Principle" section). This theory is then used in the development of a control algorithm ("Control" section) and implemented in a device prototype ("Prototype" section), which is then evaluated both theoretically and experimentally ("Prototype" section).

Working Principle

The primary function of SepaRRo is to generate a desired force $\hat{\mathbf{F}}$ at the end-effector that aims to increase the intensity of a rehabilitative training exercise or gently steer the movements of the user. This physical functionality is supported by a GUI that displays instructions to the patient, allows adjustment of therapeutic parameters, and records the performance of the patient. The force vector $\hat{\mathbf{F}}$ is the sum of two components: a desired resistive force $\hat{F}_{\parallel}$ and a desired steering force $\hat{F}_{\perp}$. The desired resistive force $\hat{F}_{\parallel}$ directly opposes the motion of the end-effector in order to increase the intensity of training. The desired steering force $\hat{F}_{\perp}$ acts perpendicularly to the direction of motion. It can be used to alter the difficulty of the training exercise by perturbing the motion away from a desired trajectory or by stabilizing it towards the trajectory. This composition can be expressed as:

$$\hat{\mathbf{F}} = \hat{F}_{\parallel}\mathbf{u}_{\parallel} + \hat{F}_{\perp}\mathbf{u}_{\perp}, \text{ with } \begin{cases} \mathbf{u}_{\parallel} = -\frac{\dot{\mathbf{x}}}{|\dot{\mathbf{x}}|} \\ \mathbf{u}_{\perp} = \begin{bmatrix} 0 & -1 \\ 1 & 0 \end{bmatrix} \mathbf{u}_{\parallel} \end{cases} \quad (1)$$

with the desired resistive force magnitude $\hat{F}_{\parallel} \geq 0$, the desired steering force magnitude $\hat{F}_{\perp} \leq 0$ or ≥ 0, and a 2D vector $\dot{\mathbf{x}}$ representing the velocity of the end-effector. The power P generated by $\hat{\mathbf{F}}$ is given by

$$P = \hat{\mathbf{F}}^T\dot{\mathbf{x}} = \left(\hat{F}_{\parallel}\mathbf{u}_{\parallel} + \hat{F}_{\perp}\mathbf{u}_{\perp}\right)^T\dot{\mathbf{x}} = -\hat{F}_{\parallel}\|\dot{\mathbf{x}}\|, \quad (2)$$

which is non-positive. This means that we should be able to rely exclusively on dissipative elements to generate a desired force $\hat{\mathbf{F}}$.

As detailed in the work of Gao and Book,[15,16] this dissipative net-power property unfortunately does not translate into the individual joints of a robotic implementation. Take, for example, the two-joint manipulator depicted in Fig. 2a. In this kinematic configuration, a downward motion $\dot{\mathbf{x}}$ of the end-ef-

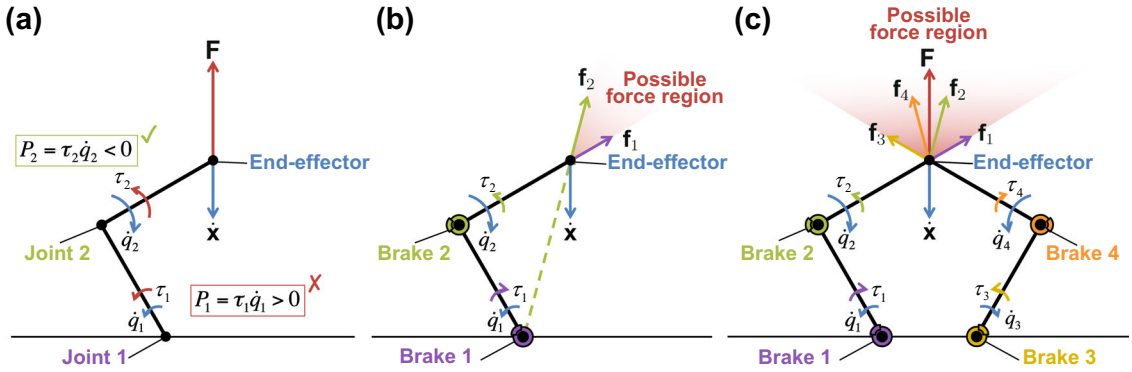

FIGURE 2. Schematic depicting the benefits of kinematic redundancy. (a) When the depicted two-joint manipulator generates a pure resistive force F against a downward motion $\dot{\mathbf{x}}$ of the end-effector, positive power P_1 is required from joint 1 (i.e., the joint torque τ_1 and the joint velocity $\dot{q}_1$ have the same sign). This happens despite the fact that the overall force at the end-effector is purely dissipative in nature. (b) When the joint torques τ_1 and τ_2 are generated by purely dissipative elements (e.g., friction brakes), they have to oppose the angular velocity at each joint ($\dot{q}_1$ and $\dot{q}_2$). This limits the possible directions of the resulting force F to the region shown in red, the conical hull of the two forces *mathbff*$_1$ and $\mathbf{f}_2$. (c) By connecting two two-link manipulators in parallel, a much larger conical hull (entire red region) can be achieved with purely dissipative elements at the joints.

fector induces a counter-clockwise angular velocity on joint 1 and a clockwise angular velocity on joint 2, i.e., $\dot{q}_1 > 0$, $\dot{q}_2 < 0$ with $\dot{\mathbf{q}}$ representing the joint velocities (shown in blue). In this configuration, a desired pure resistive force $\hat{\mathbf{F}} = \hat{F}_{\|}\mathbf{u}_{\|}$ requires counter-clockwise torques $\hat{\tau}$ from both joints: $\hat{\tau}_1, \hat{\tau}_2 > 0$ (shown in red), in which case positive power is required at joint 1, despite the net negative power at the end-effector. Please refer to the previous works for an in-depth discussion of this phenomenon.[15,16]

By limiting all joint powers to be dissipative, we can determine the range of possible forces that can be generated at the end-effector. In Fig. 2b, for example, the limitation implies that $\tau_1 \leq 0$ and $\tau_2 \geq 0$. A negative τ_1 (with $\tau_2 = 0$) generates a force in the direction of $\mathbf{f}_1$, which acts along a line that goes through joint 2, whereas a positive τ_2 (with $\tau_1 = 0$) generates a force in the direction of $\mathbf{f}_2$, which acts along a line that goes through joint 1. Thus, the generated force $\mathbf{F}$ at the end-effector must be in the conical hull of $\mathbf{f}_1$ and $\mathbf{f}_2$; i.e., $\mathbf{F} = c_1\mathbf{f}_1 + c_2\mathbf{f}_2$, where $c_1, c_2 \geq 0$ (Fig. 2b). For the given direction of motion $\dot{\mathbf{x}}$, this limits the range of achievable forces to a cone (shaded in red). The problem can be overcome partially by making the dissipative components of the manipulator redundant.[16] For example, by adding a second set of links (Fig. 2c). The generated force $\mathbf{F}$ is now a combination of four force components $\mathbf{F} = c_1\mathbf{f}_1 + c_2\mathbf{f}_2 + c_3\mathbf{f}_3 + c_4\mathbf{f}_4$, where all $c_i \geq 0$. This greatly increases the range of achievable force directions. In particular, the redundant kinematic system makes it possible to provide a pure resistive force $\hat{\mathbf{F}} = \hat{F}_{\|}\mathbf{u}_{\|}$.

Control

In order to control SepaRRo, we capture the relationship between end-effector forces/motions on one side of an equation and joint forces/motions on the other *via* the inverse kinematic function $\mathbf{q} = f_{\text{inv}}(\mathbf{x})$ that maps the Cartesian end-effector position $\mathbf{x}$ onto a vector of joint angles $\mathbf{q}$. To ensure the existence and uniqueness of this function, there have to be exactly two joints along each path from the end-effector to the ground. Additionally, we have to ensure (e.g., *via* physical hard-stops) that the system stays away from kinematic singularities (i.e., configurations when the links are fully extended or flexed) during operation. In terms of velocities, this kinematic relationship is expressed *via* the inverse Jacobian matrix $\mathbf{J}_{\text{inv}}$ that is obtained from the partial derivative of f_{inv}:

$$\dot{\mathbf{q}} = \frac{\partial f_{\text{inv}}}{\partial \mathbf{x}}\dot{\mathbf{x}} = \mathbf{J}_{\text{inv}}\dot{\mathbf{x}}. \tag{3}$$

As power is conserved between the Cartesian space and the joint space (i.e., $\mathbf{F}^T\dot{\mathbf{x}} = \tau^T\dot{\mathbf{q}}$), it follows from Eq. (3) that $\mathbf{F}^T\dot{\mathbf{x}} = \tau^T\mathbf{J}_{\text{inv}}\dot{\mathbf{x}}$ and thus:

$$\mathbf{F} = \mathbf{J}_{\text{inv}}^T\tau. \tag{4}$$

In SepaRRo, the vector of joint torques τ is generated by magnetic particle brakes. This type of brake is particularly easy to control. The torque τ_i generated by the brake on joint i is proportional to a control input $b_i \geq 0$ and opposes the angular velocity $\dot{q}_i$ of that joint:

$$\tau_i = -sgn(\dot{q}_i)b_i. \tag{5}$$

This is expressed for all joints as the vector equation $\tau = \mathbf{Sb}$, where $\mathbf{b}$ is the vector of control inputs and $\mathbf{S}$ is a diagonal matrix defined as follows:

$$\mathbf{S} = \mathrm{diag}(-sgn(\dot{\mathbf{q}})) = -\mathrm{diag}(sgn(\mathbf{J}_{\mathrm{inv}}\dot{\mathbf{x}})). \quad (6)$$

By projecting the joint torques back into Eq. (4), we get:

$$\mathbf{F} = \mathbf{J}_{\mathrm{inv}}^{\mathbf{T}}\mathbf{Sb}. \quad (7)$$

That is, for a given end-effector velocity $\dot{\mathbf{x}}$, the generated force $\mathbf{F}$ depends linearly on the control inputs $\mathbf{b}$. All achievable forces lie within the conical hull of the columns of the matrix product $\mathbf{J}_{\mathrm{inv}}^{T}\mathbf{S}$.[17]

To generate a desired force $\hat{\mathbf{F}}$, we first assumed that the desired force lies within the conical hull of $\mathbf{J}_{\mathrm{inv}}^{T}\mathbf{S}$ (Fig. 2). Because this is an under-determined equation that may have multiple solutions, we optimized the vector of control inputs $\mathbf{b}$ using the following object function and constraints:

$$\arg\min_{\mathbf{b}} \|\mathbf{b}\|_2 \text{ ,subject to } \mathbf{b} \geq 0 \text{ and } \widehat{\mathbf{F}} = \mathbf{J}_{\mathrm{inv}}^{T}\mathbf{Sb}. \quad (8)$$

Equation (8) was solved using Lagrange multipliers with duality.[2] Compared to iterative methods such as sequential quadratic programming or interior point methods, this method has the advantage of a guaranteed execution time for our real-time control application. Only if $\hat{\mathbf{F}}$ lay outside the conical hull of $\mathbf{J}_{\mathrm{inv}}^{T}\mathbf{S}$ and the constraint $\hat{\mathbf{F}} = \mathbf{J}_{\mathrm{inv}}^{T}\mathbf{Sb}$ could not be fulfilled, we applied an iterative non-negative least squares (NNLS) algorithm[27] to find the control inputs that generate a force $\mathbf{J}_{\mathrm{inv}}^{T}\mathbf{Sb}$ closest to the desired force $\hat{\mathbf{F}}$: end

$$\arg\min_{\mathbf{b}} \left\| \mathbf{J}_{\mathrm{inv}}^{T}\mathbf{Sb} - \widehat{\mathbf{F}} \right\|_2, \text{ subject to } \mathbf{b} \geq 0. \quad (9)$$

Prototype

SepaRRo was implemented as a mechanical five-bar linkage consisting of two two-joint planar manipulators connected at the end-effector (Fig. 1b).

There are a number of configurations with redundant kinematics that could be potentially applied for a semi-passive robot.[15] We employed two parallel manipulators for SepaRRo as that allowed for a wide range of steering forces within the workspace, while simultaneously keeping the device compact and portable. Other configurations, such as a five bar parallel link manipulator could allow for forces that directly resist motion, but could only supply a narrow range of steering forces.[24] A Cartesian robot may also provide resisting and steering forces without redundant kinematic structure, although this type of robot is typically larger and has a smaller workspace. The linkages for SepaRRo were manufactured from extruded aluminum U-channel profiles and mounted to a 76 cm × 76 cm acrylic table that defines the workspace. Hinges at the front of the table allowed the entire device to be tilted and operated in an inclined position (up to 70°, Fig. 1c). The two ground pivots were located 21.0 cm apart and sat 4.3 cm behind the edge of the workspace.

All links had equal lengths of 53.34 cm between pivots, with width and height of 3.81 cm and wall thickness of 0.23 cm. End stops were placed on the moving pivots to limit the range of motion and ensure the uniqueness of the inverse kinematic function f_{inv}. A bill of materials for the components of the robot can be found in Supplementary Table 1.

Each joint was actuated by a magnetic particle brake (B15, Placid Industries, Lake Placid, NY, USA), which was connected to the joint *via* a transmission with a gear ratio of 8:1 (Fig. 1b). Each brake weighed 1.1 kg and provided a torque up to $b_{\max} = 17$ N-m at the joint (measured). With these brakes in the current prototype, it is possible to achieve pure resistive forces ($\hat{F}$) ranging up to 77 N in any direction along the workspace. Many semi-passive devices have used custom electro/magnetorheological fluid brakes because they permit high torques, direct electronic control, fast actuation times, and smooth operation[19,24,35]; however cost is still prohibitive to these brakes that use "smart fluids" for actuation, and few options are available commercially. Alternatively, friction brake pads are a low-cost option capable of producing extremely high torques,[39] but these brakes are not under direct electronic control and stiction in these systems tend to make the forces unpredictable.[32]

A comparison of these various types of brakes can be found in Table 1. We note that this list is not exhaustive, and other types of brakes (e.g., eddy current brakes) could have been applied.[42] The magnetic particle brakes were chosen for this application because they are of moderate cost and provide a feeling similar to dry friction, which is a more predictable force profile. Additionally, they are under direct electronic control and have actuation times similar to smart fluid brakes (14 ms), however there is some hysteresis in the torque profile of the brake. When designing the device, in order to reduce the mass of the moving parts, the brakes on the moving pivots were located close to the ground pivots and driven *via* a timing belt transmission. Two digital encoders (A2-S-N-D-M-D, US Digital, Vancouver, WA, USA) with a resolution of 0.1° measured the joint angles q_1 and q_2 (Fig. 1b).

Using these encoders, $\dot{\mathbf{x}}$ could be calculated using the Jacobian function [Eq. (3)] for control of the robot.

TABLE 1. A comparison of various brake types.

Brake type	Advantages	Disadvantages
Magnetic particle brakes	Low cost Widely available commercially Electronically controlled Low voltage Passive and safe	Nonlinear Lower torque-to-size ratio
Electrorheological fluid brakes	Electronically controlled Passive and safe	Nonlinear Lower torque-to-size ratio Require high operating voltage (kV) Custom designed Sensitive to contamination
Magnetorheological fluid brakes	High torque-to-size rato Electronically controlled Low voltage Passive and safe	Larger and heavier Higher cost Custom designed
Friction brakes	Low cost Widely available commercially High torque-to-size ratio Passive and safe	Mechanically controlled Control requires large normal forces Stiction

This information was compiled from the authors' experience and existing works.[7,18,23,38,40]

end Due to the kinematic redundancy, no encoders were needed on the remaining joints. Forces at the end-effector were measured *via* a bi-axial load cell (MBA400, Futek, Irvine, CA, USA; 90.72 kg [200]lb] capacity) (Fig. 1b). Electrical control inputs to the brakes were supplied by a 24 V DC motor driver (SN754410, Texas Instruments, Dallas, TX, USA). The brakes were controlled *via* a pulse width modulation (PWM) signal by an Arduino UNO microcontroller that communicated *via* USB with the main computer. Communication with the encoders was done *via* USB using a SEI-to-USB adapter (SEI-USB, US Digital). The output of the load cell was amplified by an amplifier module (CSG110, Futek) and digitized *via* a DAQ device (NI USB-6218 BNC, National Instruments Corp., Austin, TX, USA), which was subsequently read by the computer *via* USB. Communication, control, and the display of the GUI was performed on a small form computer (NUC, Intel Corp., Santa Clara, CA, USA; Processor: Intel i7-5557U; RAM: 16GB), which ran custom code developed by our group. This control software was implemented in Python, running in four threads with an update frequency of ~66.4 Hz. A main thread rendered the GUI and calculated the control input according to Eqs. (8) and (9). The GUI included a graphical representation of the workspace that showed the end-effector's current position as well as the target positions of the current motion. Upon completing each trial, the operator was given the option to save and display trial data, which included the positions, velocities, and load cell readings as a function of time. The main thread was supported by a kinematics thread that read the joint angles q_1 and q_2 from the encoders and calculated $\mathbf{x}$, q_3 and q_4, as well as the derivatives $\dot{\mathbf{q}} = \frac{\Delta \mathbf{q}}{\Delta t}$ and $\dot{\mathbf{x}} = \boldsymbol{J}\dot{\mathbf{q}}$; by a driver thread that computed and sent PWM signals to the motor drivers to actuate the brakes; and by a sensor thread that recorded the value of the measured force at the end-effector.

Evaluation

We evaluated the performance of SepaRRo using theoretical analyses, hardware experiments, and testing on healthy human subjects. In particular, we evaluated SepaRRo's ability to generate a range of resistance patterns and quantified the accuracy of the generated forces. Furthermore, we evaluated muscle activation patterns while using the device.

Theoretical Analyses

All theoretical analyses were performed using a high performance computer (Z840, HP, Palo Alto, CA, USA; Processor: 2× Intel Xeon E5-2687W v4, Cores: 48, RAM: 64GB), and took approximately 120hrs to run to completion. To assess the theoretical limits of our design and controller, we computed two performance metrics at each position within the end-effector's workspace: the minimum of maximum force $\breve{F}(\mathbf{x})$ and minimum of maximum steering angle $\breve{\alpha}(\mathbf{x})$. At a given end-effector position $\mathbf{x}$, $\breve{F}(\mathbf{x})$ is defined as the minimum value among the maximally achievable resistive force magnitudes $F_{\|,\max}(\mathbf{x}, \underline{\mathbf{x}})$ for all possible directions of motion $\dot{\mathbf{x}}$. This force magnitude is limited

by the kinematics and by the saturation of the brakes that limits $b_i \leq b_{\max}$:

$$\begin{aligned} &\breve{F}(\mathbf{x}) = \min\left(F_{\parallel,\max}(\mathbf{x},\underline{\mathbf{x}})\right) \\ &\text{s.t. } \mathbf{b} \text{ is the solution of Eq.(9) for } \hat{\mathbf{F}} = F_{\parallel,\max}\mathbf{u}_{\parallel} \\ &F_{\parallel,\max}\mathbf{u}_{\parallel} = \mathbf{J}_{\text{inv}}^{\mathbf{T}}\mathbf{S}\mathbf{b} \\ &\max(\mathbf{b}) = b_{\max}. \end{aligned} \tag{10}$$

That is, it is guaranteed that the device can provide a pure resistive force with a magnitude of at least $\breve{F}(\mathbf{x})$ at the position $\mathbf{x}$, regardless of the velocity $\dot{\mathbf{x}}$. Similarly, the achievable steering angle varies according to the position and the direction of motion of the end-effector. At a given end-effector position $\mathbf{x}$, $\breve{\alpha}(\mathbf{x})$ is defined as the minimum value among the maximally achievable steering angles $\alpha_{\max}(\mathbf{x},\underline{\mathbf{x}})$ for all possible directions of motion $\dot{\mathbf{x}}$:

$$\begin{aligned} &\breve{\alpha}(\mathbf{x}) = \min(\alpha_{\max}(\mathbf{x},\underline{\mathbf{x}})) \\ &\text{s.t. } \alpha_{\max}(\mathbf{x},\underline{\mathbf{x}}) = \max_{\mathbf{f}}\left(\cos^{-1}\left(\frac{-\mathbf{f}\cdot\underline{\mathbf{x}}}{\|\mathbf{f}\|\cdot\|\underline{\mathbf{x}}\|}\right)\right) \\ &\quad \mathbf{f} = \mathbf{J}_{\text{inv}}^{\mathbf{T}}\mathbf{S}\mathbf{b} \\ &\quad \mathbf{b} \text{ is the solution of Eq.(9) for } \hat{\mathbf{F}} = \mathbf{f}. \end{aligned} \tag{11}$$

That is, it is guaranteed that the device can provide a steering angle of at least $\breve{\alpha}(\mathbf{x})$ at the position $\mathbf{x}$, regardless of the velocity $\dot{\mathbf{x}}$. Both values of $\breve{F}$ and $\breve{\alpha}$ are ideally as large as possible.

To provide a baseline for the achievable performance, we first quantified the theoretical ability to generate forces over the range of the device's workspace. To this end, we computed $\breve{F}(\mathbf{x})$ and $\breve{\alpha}(\mathbf{x})$ [as defined in Eqs. (10) and (11)] over a dense grid of locations $\mathbf{x}$, distributed across the device's entire workspace. Additionally, we computed the maximum pure resistive force and maximum steering angle for motions in the eight cardinal and inter-cardinal directions (i.e., $\angle\dot{\mathbf{x}} = 0°, 45°, 90°, 135°, 180°, 225°, 270°, 315°$, with $\angle\dot{\mathbf{x}}$ being the angular component of the polar coordinates of the velocity vector).

Hardware Experiments

We then experimentally verified the ability of SepaRRo to generate desired forces within the workspace. In order to obtain clean data, great care was taken to move the end-effector with constant velocity along defined paths. To this end, the end-effector was pulled along a straight edge using an inelastic cable that was wound up on a pulley driven by a constant velocity motor (approximately 0.71 m/s). With this setup, two sets of experiments were conducted: (1) we tested SepaRRo's ability to generate desired pure resistive forces $\hat{F}_{\parallel}$, and (2) we tested SepaRRo's ability to generate desired steering forces $\hat{F}_{\perp}$. All experiments were performed by moving the end-effector between six targets located within the workspace (Fig. 1d). Target 0 was located at the bottom center of the work space: $\mathbf{t_0} = \begin{bmatrix} \mathbf{0} \\ \mathbf{0} \end{bmatrix}$. Targets 1–5 were distributed around $\mathbf{t_0}$ along an ellipse with a vertical axis of 0.57 m and a horizontal axis of 0.38 m, at an angle of 0°, 45°, 90°, 135°, and 180°. That is, $\mathbf{t_1} = \begin{bmatrix} \mathbf{0.38} \\ \mathbf{0} \end{bmatrix}$, $\mathbf{t_2} = \begin{bmatrix} \mathbf{0.32} \\ \mathbf{0.32} \end{bmatrix}$, $\mathbf{t_3} = \begin{bmatrix} \mathbf{0} \\ \mathbf{0.57} \end{bmatrix}$, $\mathbf{t_4} = \begin{bmatrix} \mathbf{-0.32} \\ \mathbf{0.32} \end{bmatrix}$, $\mathbf{t_5} = \begin{bmatrix} \mathbf{-0.38} \\ \mathbf{0} \end{bmatrix}$, The notation $A \rightarrow B$ described the linear path from target A to target B. Experiments were performed over a range of resistive force magnitudes.

1. To test SepaRRo's ability to generate desired pure resistive forces $\hat{F}_{\parallel}$, we pulled the end-effector along paths $0 \rightarrow 1$, $0 \rightarrow 2$, $0 \rightarrow 3$, $0 \rightarrow 4$, $0 \rightarrow 5$, $1 \rightarrow 0$, $2 \rightarrow 0$, $3 \rightarrow 0$, $4 \rightarrow 0$, and $5 \rightarrow 0$. For each motion, SepaRRo was commanded to generate a force $\hat{\mathbf{F}}$ with $\hat{F}_{\parallel} = 0$, 8, 16, 24, and 32 N and $\hat{F}_{\perp} = 0$. We recorded the direction and magnitude of the generated actual force $\mathbf{F}$ for each of these 50 experiments.
2. To test SepaRRo's ability to generate desired steering forces $\hat{F}_{\perp}$, we pulled the end-effector along paths $0 \rightarrow 1$, $0 \rightarrow 2$, $0 \rightarrow 3$, $0 \rightarrow 4$, $0 \rightarrow 5$, $1 \rightarrow 0$, $2 \rightarrow 0$, $3 \rightarrow 0$, $4 \rightarrow 0$, and $5 \rightarrow 0$. For each motion, SepaRRo was commanded to generate a force $\hat{\mathbf{F}}$ of 16 N magnitude directed at 45° to the left and to the right of the pure resistive direction (i.e. $\hat{F}_{\parallel} = 8\sqrt{2}N$ and $\hat{F}_{\perp} = \pm 8\sqrt{2}N$). We recorded the direction and magnitude of the generated actual force $\mathbf{F}$ for each of these 20 experiments.

Human Subjects Experiment

Finally, we conducted a human subjects experiment in order to provide insight into the physiological effects of performing resisted reaching with SepaRRo. Six healthy subjects (gender: male, age: 25.83 ± 7.14 years, height: 180.83 ± 11.32 cm, weight: 74.88 ± 16.71 kg) participated in this study. All participants signed an informed consent document that was approved by the University of Michigan Institutional Review Board. For this evaluation, wireless surface electromyography (EMG) electrodes (Trigno, Delsys, Inc., Natick, MA, USA) were placed on the skin overlying the pectoralis major (clavicular), pectoralis major (sternal), latissimus dorsi, deltoid, biceps brachii, brachioradialis, triceps brachii, wrist flexors, and wrist extensors. Prior to the experiment, maximum voluntary contractions

(MVCs) for each of these muscles were recorded while the experimenter manually imposed a resistance on the subjects. EMG signals were recorded during each trial while the subjects were seated with target 0 aligned with their sternum and held the handle mounted on the end-effector and moved it between the target positions. To this end, the subjects were shown the start and end targets *via* the GUI and were given visual feedback about the current end-effector position. With this set-up, the subjects were instructed to move the device from $0 \rightarrow 2$, $0 \rightarrow 3$, $0 \rightarrow 4$, $0 \rightarrow 5$, $2 \rightarrow 0$, $3 \rightarrow 0$, $4 \rightarrow 0$, and $5 \rightarrow 0$. We excluded the $0 \rightarrow 1$ and $1 \rightarrow 0$ paths as these data were redundant with the $0 \rightarrow 5$ and $5 \rightarrow 0$ paths. Additionally, the muscle activation profiles were very similar along these redundant reaching paths (average difference $< 1\%$ of MVC). These trials were performed at three levels of a pure resistive force ($F_{\perp} = 0$): $F_{\parallel} = 0$, 16, and 32 N. We also performed steering trials, where the subjects performed a forward reach from $0 \rightarrow 3$ and off-axis steering forces (i.e., $F_{\perp} \neq 0$) of 16 and 32 N were directed 45° to the left and to the right of the pure resistive direction. Steering trials were performed to evaluate whether selective groups of muscles can be targeted while training with SepaRRo (e.g., targeting the deltoid and triceps brachii muscles during resisted reaching by providing a steering force directed to the left or targeting pectoral muscles and biceps brachii by providing a steering force to the right). Alternatively, the steering trails could act as a disturbance to perturb the user from an intended path. During each trial, the force measured from the load cell and the raw EMG signals were sampled at 1000 Hz using our custom built software written in LabVIEW 2011 (National Instruments Corp., Austin, TX, USA).

Raw EMG data were band-pass filtered (20–500 Hz), rectified, and smoothed using a zero-phase-lag, low-pass Butterworth digital filter (8th order, 6 Hz cut-off).[42] The resulting EMG profiles were normalized to their MVC values in order to express muscle activation as a percentage of the subjects' maximum ability. We then calculated the average muscle activation over each trial by detecting the onset and offset of force through the load cell and calculating the average of the EMG over this window. For the purely resistive trials, these EMG values were then represented as vectors in polar coordinates $(R_{\mathrm{EMG}}, \theta)$ and were evaluated by computing the principal direction of muscle action and specificity index (i.e., how focused is the muscle's activity along its principal direction) using circular statistics.[11,25,41,45] The principal direction (ϕ) of muscle action was computed using the following formulae:

$$\mathbf{v_i} = \begin{bmatrix} v_{\mathrm{xi}} \\ v_{\mathrm{yi}} \end{bmatrix} = \begin{bmatrix} R_{\mathrm{EMGi}} \cos(\theta_i) \\ R_{\mathrm{EMGi}} \sin(\theta_i) \end{bmatrix} \tag{12}$$

$$\phi = \arctan\left(\frac{\sum_{i=1}^{8} v_{\mathrm{yi}}}{\sum_{i=1}^{8} v_{\mathrm{xi}}}\right), \tag{13}$$

where i indicates each trial performed along different reaching directions at each force intensity. Muscle specificity index was expressed by the ratio of the magnitude of the resultant EMG vector to the sum of the magnitudes of EMG vector along each direction, i.e.,

$$\text{Specificity Index} = \frac{\left\| \sum_{i=1}^{8} \mathbf{v_i} \right\|}{\sum_{i=1}^{8} \left\| \mathbf{v_i} \right\|} \tag{14}$$

Specificity index is a scalar that ranges between 0 and 1, with 0 representing that the muscle is active in all directions equally and 1 representing that the muscle is active in only one direction (i.e., along the principal direction). Typically, when muscle activity is low (i.e., at noise level) or the muscle is co-contracting (i.e., working to stabilize the movement) specificity index would be low, in which case the principal direction has to be interpreted with caution. The principal directions and muscle specificity indices were averaged across trials (16 and 32 N) for each muscle and were compared with the muscle's expected anatomical angle of action (pectoralis major = 180°, deltoid = 0°, biceps brachii and brachioradialis = 225°, triceps brachii = 45°). We did not expect anatomical angle of action for latissimus dorsi and wrist flexors/extensors, because these muscles were expected to co-contract along several directions to stabilize the movement.

Statistical Analysis

Statistical analyses were performed on the EMG data to detect significant changes in muscle activation during the purely resistive and steering trials of the human subjects experiment. All statistical analyses were performed using SPSS for windows version 22.0 (SPSS Inc., Chicago, IL, USA). Descriptive statistics were calculated for each variable. Prior to statistical analysis, all EMG data were log transformed ($\log_e$EMG) to minimize skewness and heteroscedasticity.[12,26] For the purely resistive trials, we performed linear regressions for each muscle with summed EMG (denominator of the specificity index equation)[25] as the dependent variable and force level as the independent variable. To evaluate changes in muscle activation due to steering, we

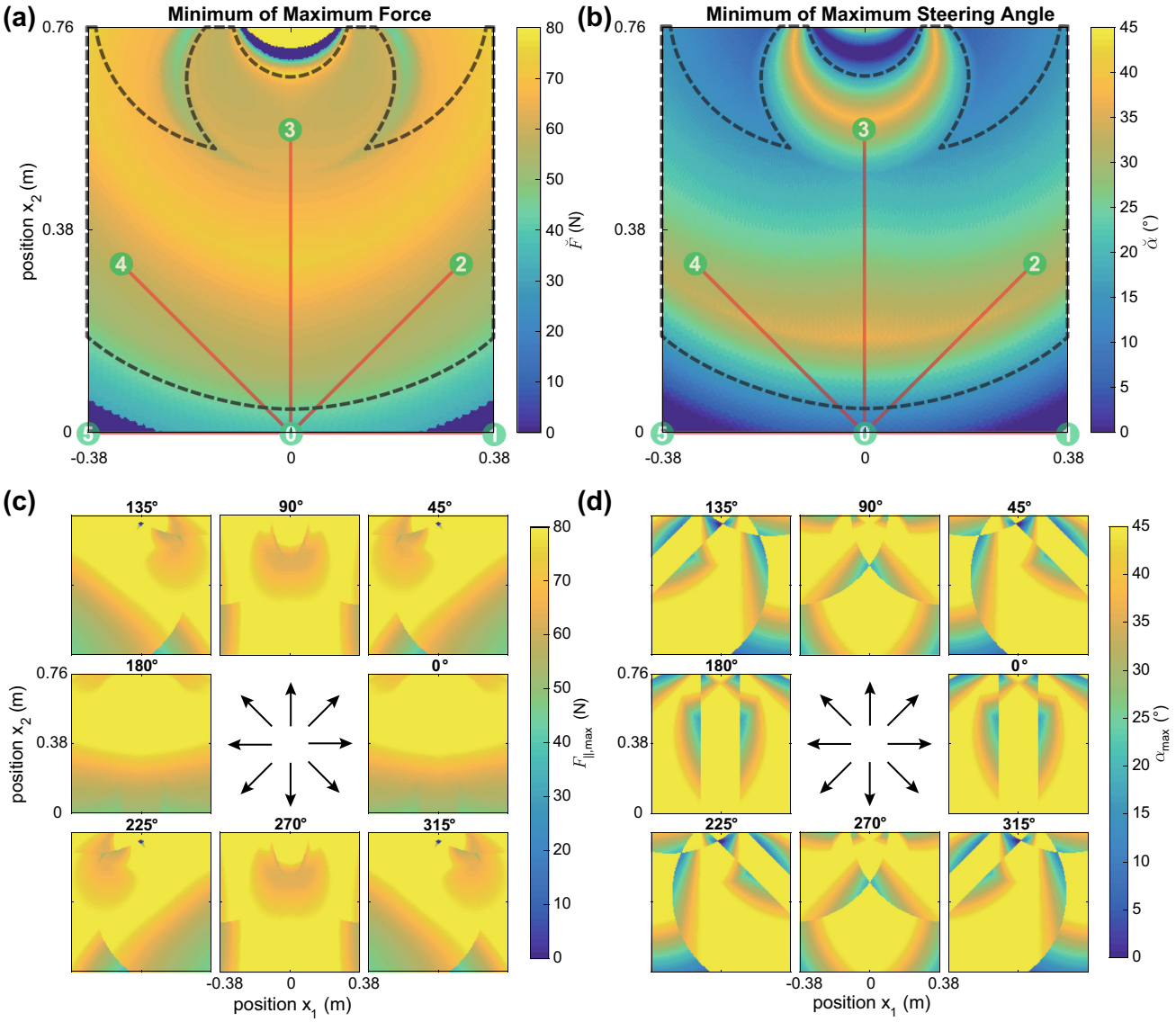

FIGURE 3. (a) Minimum of maximum force ($\breve{F}$) and (b) minimum of maximum steering angle ($\breve{\alpha}$) are shown as functions of the position of the end-effector within the workspace. The two plots show the performance of SepaRRo when generating these purely resistive forces or steering angles independent of the direction and magnitude of the end-effector velocity. Inside the dashed lines (covering about 80% of the entire workspace) the end-effector can generate at least 45 N of pure resistive force and create a steering angle of at least 15°. The numbers 0–5 denote the location of the 6 targets used in the validation experiments (hardware and human subject). Note that even in areas where the theoretical force values are 0 N, SepaRRo is capable of generating large forces; however, these forces will not be purely resistive and will have a slight steering effect. (c) Maximally achievable resistive force magnitudes $F_{\|,\max}$ and (d) maximally achievable steering angles $\alpha_{\max}$ for motions in the eight cardinal and inter-cardinal directions. Since the end-effector only moves in one direction, the values of achievable resistive force and steering angle seen here are larger than those shown in (a) and (b).

performed repeated measures analysis of variance (ANOVA) with force level (two levels: 16 and 32 N) and force direction (two levels: purely resistive and steering) as within-subjects factors. The magnitudes of EMG activity observed during straight and steering trials were used as the dependent variable. The steering direction (i.e., to the left or right of the purely resistive force) used for each muscle was determined based on the principal direction ϕ for that muscle (e.g., the pectoralis major muscles have ϕ pointing to the left, and were analyzed with the rightward steering force; whereas the deltoid has ϕ pointing to the right, and was analyzed with the leftward steering force). Significant force direction (i.e., steering) and force level × force direction interaction effects were followed by *post hoc* analyses using paired t-tests with Bonferroni correction for multiple comparisons. A significance level of $\alpha = 0.05$ was used for all statistical analyses.

BMES BIOMEDICAL ENGINEERING SOCIETY™ www.bmes.org

TABLE 2. Error in force magnitude and force direction during the hardware experiment for a purely resistive force ($\hat{F}_\perp = 0$), averaged over four different values (excluding 0 N) of $\hat{F}_\parallel$.

Path	0 → 5	0 → 4	0 → 3	0 → 2	0 → 1
Error (magnitude [N]):	− 0.59 ± 0.24	1.54 ± 0.80	0.46 ± 0.71	0.44 ± 0.75	− 0.50 ± 0.66
Error (direction [°]):	8.9 ± 6.7	− 17.5 ± 8.8	16.1 ± 8.0	11.6 ± 9.4	− 22.9 ± 2.5
Path	1 → 0	2 → 0	3 → 0	4 → 0	5 → 0
Error (magnitude [N]):	0.45 ± 0.32	− 1.94 ± 0.28	1.17 ± 1.71	0.08 ± 0.53	1.55 ± 0.54
Error (direction [°]):	− 30.0 ± 11.0	1.1 ± 3.4	− 13.9 ± 8.0	− 2.6 ± 3.5	16.2 ± 10.3

RESULTS

Theoretical Limitations

The results of the numerical computation of $\breve{F}(\mathbf{x})$ and $\breve{\alpha}(\mathbf{x})$ are shown as heat maps in Figs. 3a and 3b. With the specific kinematic structure and with the limitations of our brakes ($b_{\max} = 17$ N-m), $\breve{F}(\mathbf{x})$ ranged from 0 N to about 80 N and $\breve{\alpha}(\mathbf{x})$ ranged from 0° to 45°. Both achievable force and achievable steering angle were strongly dependent on the position of the end-effector within the workspace. In about 80% of the workspace, the end-effector generated a pure resistive force of at least 45 N and a steering angle of at least 15°—regardless of the magnitude or direction of the end-effector motion. Note that the maximally achievable force magnitude scales linearly with the capacity of the brakes (i.e., with $b_{\max}$), whereas the steering angle is only dependent on the kinematic structure of the manipulator and cannot be increased by brakes with a higher torque capacity.

The values of $\breve{F}(\mathbf{x})$ and $\breve{\alpha}(\mathbf{x})$ give a conservative estimate of the ability of SepaRRo, and show its capacity for the worst possible direction of motion at each location.

Estimates for $\breve{F}(\mathbf{x})$ are also largely dependent on $b_{\max}$, and can be altered with different brakes or gearing ratios. Thus, these values greatly underestimate the device's ability when it is moving in a particular direction. Figures 3c and 3d show heat maps of the maximum force and maximum steering angle when the end-effector is pushed in the eight cardinal and inter-cardinal directions. In these directions, the end-effector generated a pure resistive force of at least 60 N and a steering angle of at least 34° in about 80% of the workspace. Thus, if subjects are performing straight line reaching in these directions, as is done in many rehabilitation practices, the device can exceed its fundamental theoretical limitations.

Hardware Experiments

The force data recorded during the hardware experiments were averaged individually for each trial and standard deviations were computed. For the trials with a desired pure resistive force ($\hat{F}_\perp = 0$), the resulting mean values and standard deviations are shown as polar plots in Fig. 4 for motions away from the origin and in Fig. 5 for motions towards the origin. The desired force magnitudes were achieved with high precision; however, at a setting of 0N only, a small systematic error of 3.5 N was visible (mean error, averaged across all 10 trials with $\hat{F}_\parallel = 0$). This systematic error likely stems from residual torques in the brakes, as well as from friction in the mechanical linkage. There was also some asymmetrical behavior of the robot, particularly when moving between targets $0 \rightarrow 1$ and $0 \rightarrow 5$. Given that the robot is symmetrical, we would have expected to have the same behavior for each of these trials. This could have been due to subtle asymmetries in the robots design, such as slight variation in brake calibrations or friction in joints. However, during use, it is difficult for the subject to perceive these errors. When averaged across all other 40 trials, the mean error was 0.27 ± 1.23 N. Overall, the generated force magnitudes were also very consistent. The average of the standard deviation of all 50 trials was 1.00N. The direction of the generated force vectors showed greater errors and a stronger dependency on the path of motion. Table 2 shows the average error in force magnitude and direction for each of the 10 evaluated paths.

For the trials with a desired steering force ($\hat{F}_\perp = \pm\hat{F}_\parallel$), the resulting mean values and standard deviation are shown as polar plots in Fig. 6. The average generated force magnitude across all of these 20 trials was 15.20 ± 3.21 N (commanded value: 16N), and the average error of the generated force angle was $0.3 \pm 12.8°$. Errors in the steering angle could have arose because we commanded the robot to provide an angle of 45°, where this angle is not obtainable over the entire workspace. However, the robot attempted to minimize these errors to provide the maximum possible steering angle.

Human Subjects Experiment

Muscle activation patterns during various force contractions are plotted as polar plots (Fig. 7). In general, the magnitude of muscle activity increased as

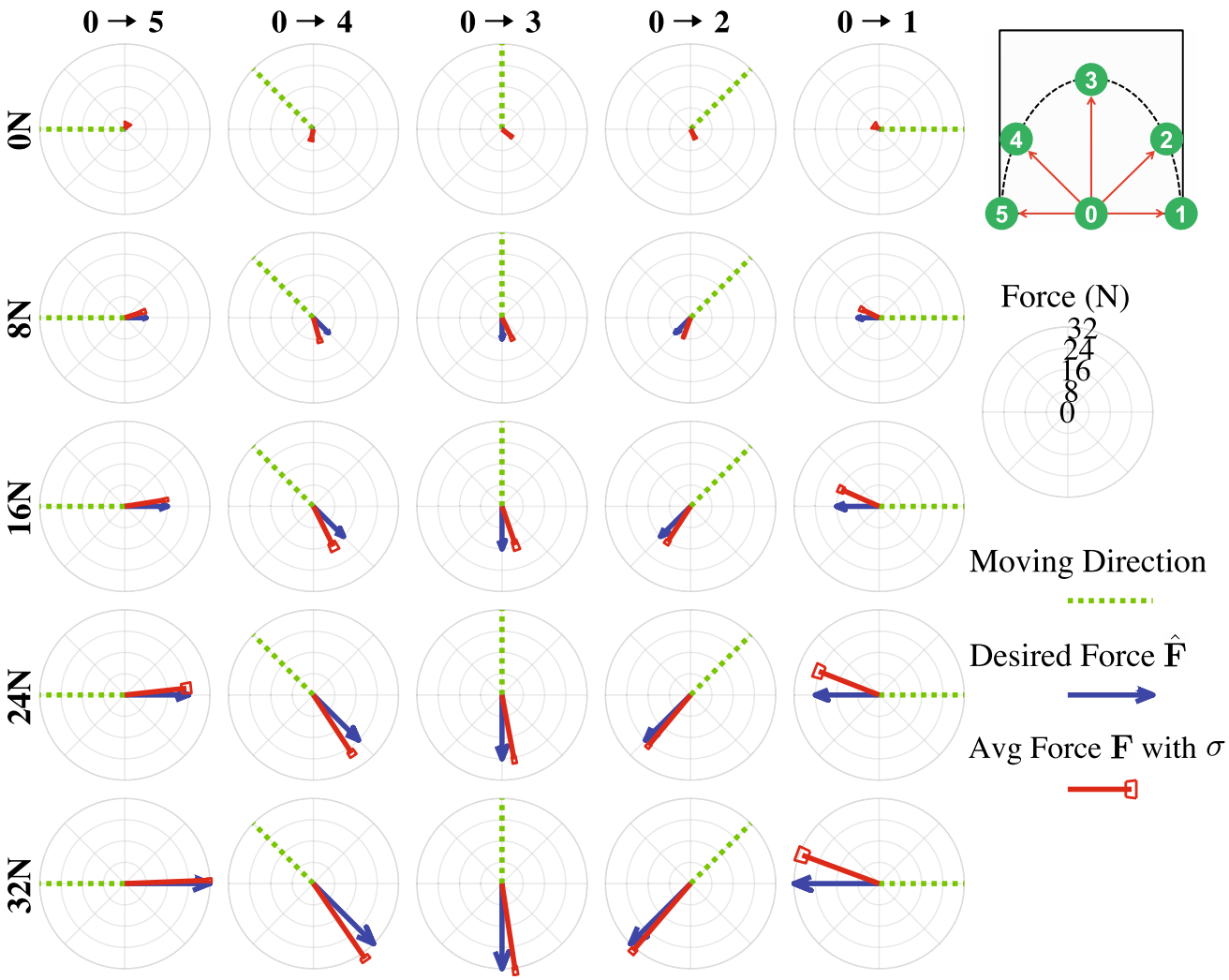

FIGURE 4. Polar plots depicting the average force vectors obtained for each individual hardware trial as the end-effector of SepaRRo was pulled using a constant velocity motor from the origin (target 0) towards targets 1–5. The desired force $\hat{F}$ was directly opposing the motion with force magnitudes ranging from 0 to 32 N.

the force level increased. Muscle specificity indices ranged from 0.04 to 0.47, with low specificity indices observed in the 0N force condition.

The principal direction of muscle action for all of the muscles were close (5.11° to 24.33° of error) to the muscles' predicted anatomical angle of action (Table 3). Linear regression indicated that all muscles increased their activation when scaling resistance of the robot except for the latissimus dorsi ($e^{\beta} = 1.020$ to 1.045, $p < 0.001$ to 0.048). Force data from the purely resistive trials are shown in Table 4.

During steering trials, when subjects performed a forward reaching motion (i.e., $0 \rightarrow 3$) with an off-axis steering forces applied, we found that many muscles that were previously inactive during this motion greatly increased in activation (Fig. 8). This was shown by significant steering × force level interactions for pectoralis major (clavicular) [$F(1, 5) = 11.293$, $p = 0.020$], pectoralis major (sternal) [$F(1, 5) = 85.729$, $p < 0.001$], and deltoid muscles [$F(1, 5) = 7.890$, $p = 0.038$]. *Post hoc* analysis indicated that activation was higher in these muscles during the steering trials at both force levels, but to a greater extent at the 32N level ($p = 0.003$ to 0.030) than at the 16N level. Significant steering effects were also seen in the biceps brachii [$F(1, 5) = 8.249$, $p = 0.035$], triceps brachii muscle [$F(1, 5) = 14.673$, $p = 0.012$], and wrist flexor muscles [$F(1, 5) = 22.938$, $p = 0.005$], where *post hoc* testing showed higher triceps brachii and wrist flexors muscle activation at both force levels ($p = 0.002$ to 0.021) and higher biceps brachii activation at the 32N level during steering trials ($p = 0.04$). During steering trials, we measured average forces of 16.73 ± 3.25 and 33.95 ± 4.53 N for the low and high force levels, respectively.

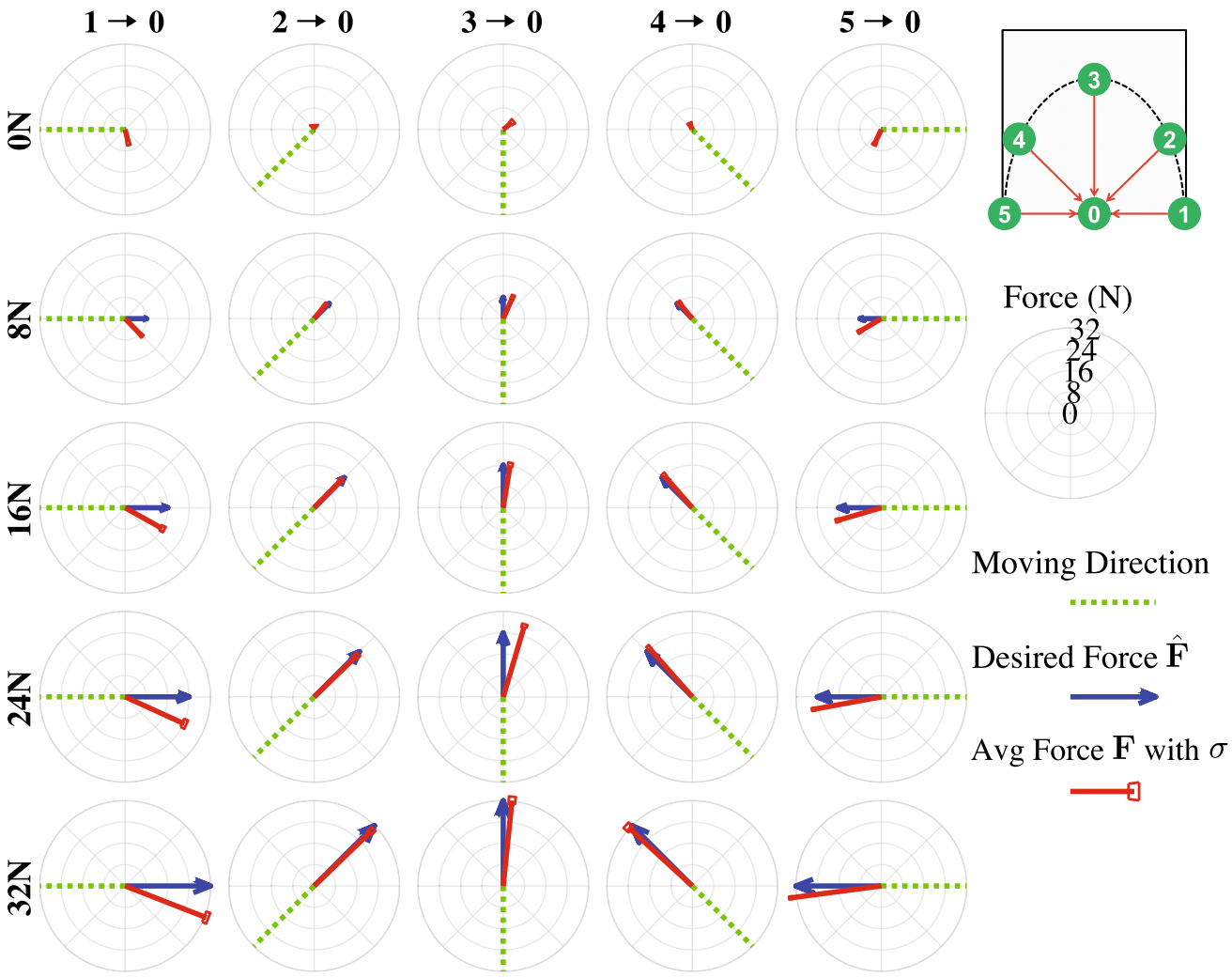

FIGURE 5. Polar plots depicting the average force vectors obtained for each individual hardware trial as the end-effector of SepaRRo was pulled using a constant velocity motor from targets 1–5 towards the origin (target 0). The desired force $\hat{F}$ was directly opposing the motion with force magnitudes ranging from 0 to 32 N.

DISCUSSION

In this paper, we introduce SepaRRo: a semi-passive rehabilitation robot aimed at providing functional resistance training for upper extremities during reaching. Unlike traditional assistive robots that use motors, SepaRRo operates using magnetic particle brakes in order to make it cost-effective, safe, and portable, which are critical elements for in-home rehabilitation programs. Moreover, the robot improves upon current low-cost passive devices (e.g., elastic bands and free weights) because it is controllable, which allows us to program unique force environments for the user and scale resistance based on their ability level. To verify these claims, we carefully designed, implemented, and tested a prototype through both theoretical analyses and hardware experiments. We also applied SepaRRo in a human subjects experiment on healthy subjects to demonstrate how variable intensity resistive and steering forces modulate muscle activity during reaching.

Our numerical analysis and hardware experiments using the SepaRRo prototype indicated that the robot can provide scalable and steerable resistances over most of the 76 × 76 cm^2 workspace tested in this study. Numerical analyses also confirmed that the current configuration of the robot (link lengths, brakes, base joint spacing) can provide the user with a pure resistive force (i.e., directly opposite to the intended movement direction) of at least 45 N and a steering angle of at least 15° within approximately 80% of the workspace, regardless of the velocity (magnitude and direction) of the end-effector. The regions of the workspace in which the robot was unable to meet these criteria primarily occurred when the robot was in configurations that approached singularities (i.e., the linkages were

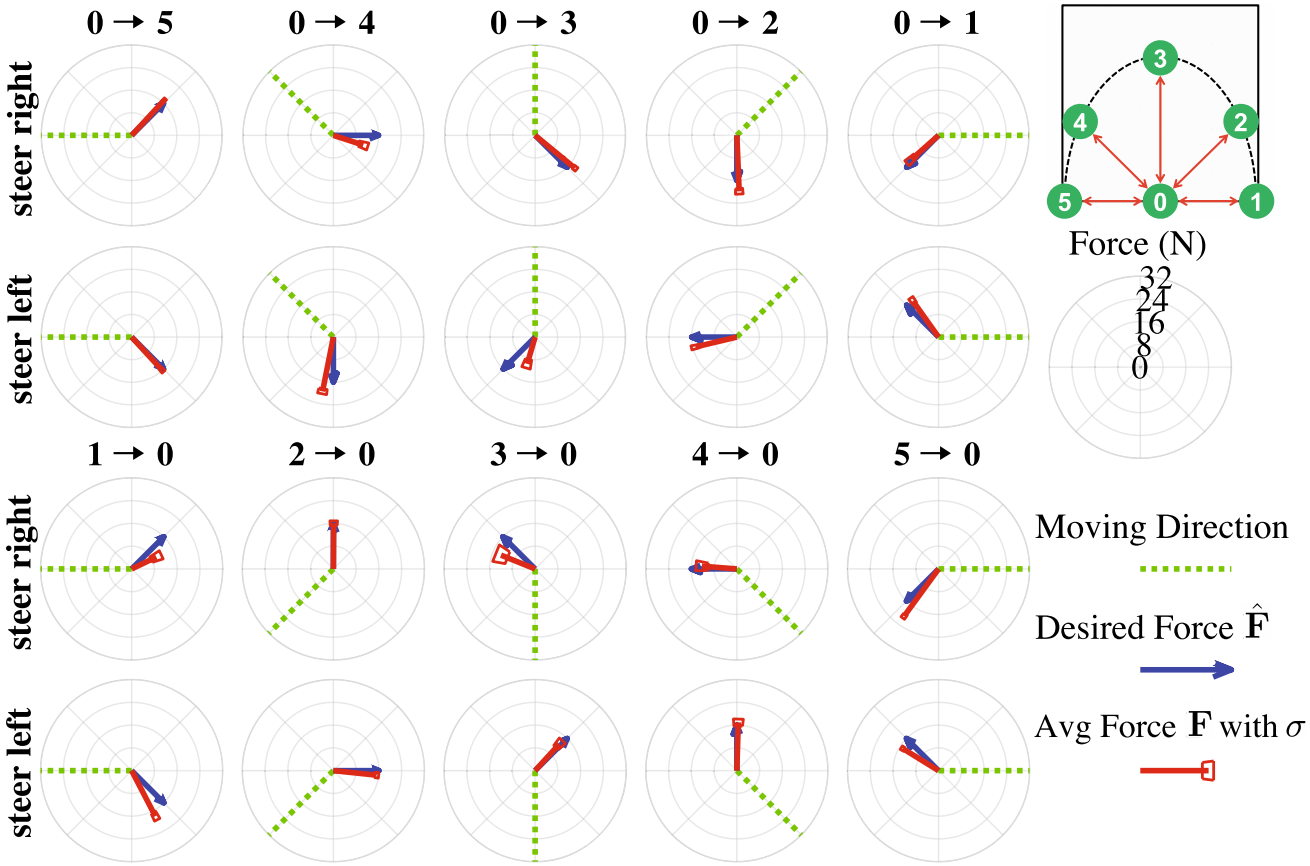

FIGURE 6. Polar plots depicting the average force vectors obtained for each individual hardware trial as the end-effector of SepaRRo was pulled using a constant velocity motor from target 0 towards targets 1–5 (top rows) and from targets 1–5 towards target 0 (bottom rows). The desired force $\hat{F}$ was acting at a 45° angle to either the left or the right of the direction of motion (i.e., steering), with a force magnitude of 16 N.

TABLE 3. Average principal direction and specificity index of various upper-extremity muscles during directional reaching.

Muscle	Expected angle	Principal direction (ϕ) (°)	Specificity index
Pectoralis major (clavicular)	180°	171.52 ± 11.34	0.34 ± 0.11
Pectoralis major (sternal)	180°	174.89 ± 10.34	0.32 ± 0.18
Latissimus dorsi	NA	135.07 ± 68.75	0.29 ± 0.07
Deltoid	360°	353.78 ± 19.42	0.37 ± 0.13
Biceps brachii	225°	236.94 ± 9.35	0.41 ± 0.08
Brachioradialis	225°	249.33 ± 56.05	0.19 ± 0.10
Triceps brachii	45°	61.54 ± 47.67	0.27 ± 0.14
Wrist flexors	NA	217.98 ± 11.83	0.25 ± 0.09
Wrist extensors	NA	163.37 ± 104.27	0.20 ± 0.11

near full extension at the bottom of the workspace or full flexion towards the top). It is important to note that these values are very conservative, and performance only degraded for very specific directions of motion in these areas. When repeating our numerical analysis for motions in the eight cardinal and intercardinal directions (as is typically done during therapy), the robot provided 60 N of purely resistive force and 34° of steering within 80% of the workspace (Figs. 3c and 3d).

These findings were mostly corroborated through physical testing of the device, where the end-effector was driven using a constant velocity motor along a straight edge. Here, we saw that, on an average, the robot was able to consistently provide pure resistive forces of up to 32N accurately (average error of

TABLE 4. Average force measured during the human subjects experiment

Desired force (N)	Measured force (N)				
Path	0 → 5	0 → 4	0 → 3	0 → 2	0 → 1
0	3.52 ± 0.73	5.81 ± 0.84	5.98 ± 0.70	5.03 ± 0.77	6.84 ± 2.17
16	18.74 ± 1.97	18.81 ± 2.53	17.36 ± 3.64	17.57 ± 2.95	18.67 ± 2.91
32	29.85 ± 9.42	32.85 ± 3.94	32.68 ± 5.54	30.90 ± 8.37	32.07 ± 3.86
Path	1 → 0	2 → 0	3 → 0	4 → 0	5 → 0
0	6.32 ± 0.81	4.94 ± 2.45	5.79 ± 2.28	5.65 ± 3.33	4.18 ± 1.84
16	19.35 ± 3.15	17.20 ± 3.29	19.88 ± 4.41	15.87 ± 4.46	13.83 ± 6.56
32	32.14 ± 3.91	34.92 ± 6.12	38.69 ± 6.07	31.35 ± 6.30	30.75 ± 5.05

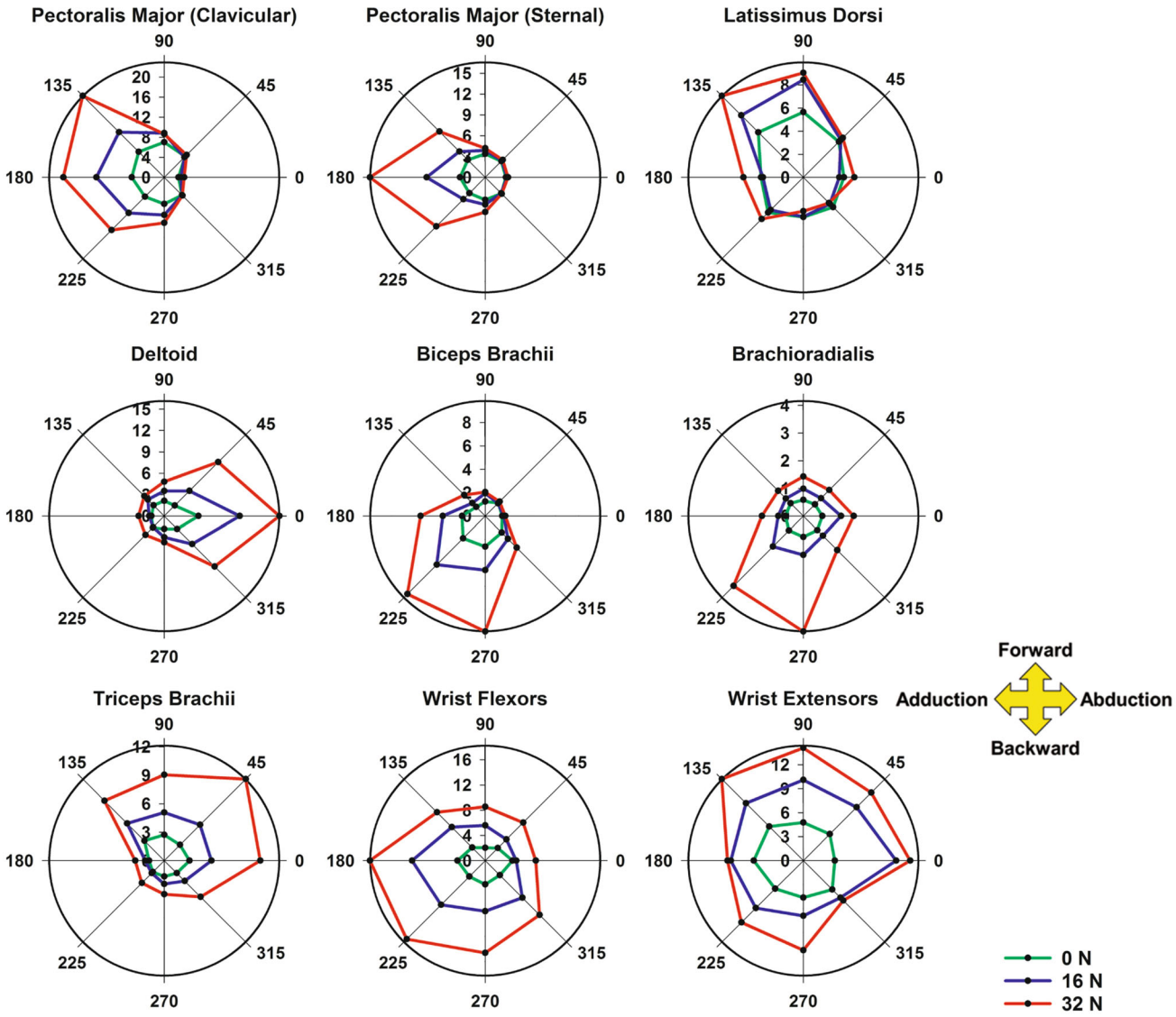

FIGURE 7. Polar plots depicting muscle activation of various upper-extremity muscles during directional reaching. The amplitude of muscle activation (% MVC) as measured using EMG are plotted with the direction (°) that the subjects were reaching for each force condition. Arrows in the legend show the anatomical action of the reaching movement.

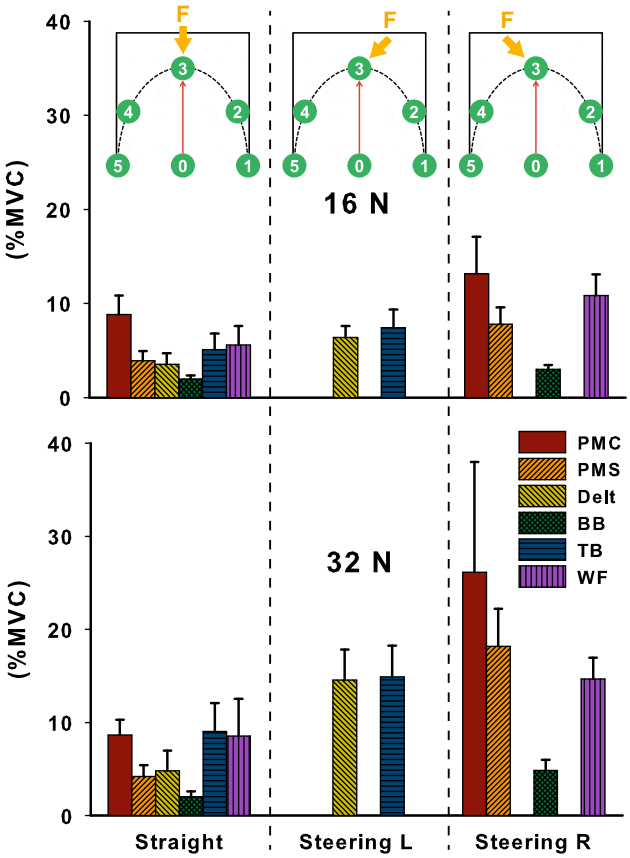

FIGURE 8. Bar graphs depicting average muscle activation during straight and steering trials. The top panel indicates the direction of the movement and the force direction (F). PMC: pectoralis major (clavicular), *PMS* pectoralis major (sternal), *Delt* deltoid, *BB* biceps brachii, *TB* triceps brachii, *WF* wrist flexors. Note that only muscles that showed a significant ($p < 0.05$) difference between straight and steering trials are plotted.

magnitude: 0.27 ± 1.23 N, average error of angle: $-3.3 \pm 17.6°$ across 40 non 0 N trials). Furthermore, the robot was able to achieve a 45° steering angle accurately (average error of angle: $0.3 \pm 12.8°$ across the steering trials) along the reaching paths. On an individual trial level, there were some errors and asymmetries that arose based on the movement direction, and these could be due to the implementation (e.g., joint friction) or experimental setup when using this early prototype. Overall, the robot showed a high level of competence when providing large purely resistive or steering forces. We expect that these features of SepaRRo would be useful in rehabilitation, as they would allow therapists to tailor treatment based on the patient's impairment and ability level. However, further testing in a patient population is required to verify the clinical potential of the device.

Manipulation of the force characteristics of the robot also lead to measurable changes in muscle physiology. Specifically, we saw a notable increase in muscle activation of the pectoralis major, deltoid, biceps brachii, brachioradialis, triceps brachii, wrist flexors, and wrist extensors—a wide variety of both proximal and distal muscles. Further, the patterns of muscle activation scaled with the resistance levels. Thus, SepaRRo could provide a potentially affordable means to engage the upper extremity muscles during training. We also saw that many of these muscles had marked principal directions (ϕ) that were similar to their anatomical angle of action. Hence, if the robot was set to provide resistance along these principal directions, rehabilitation could be applied in a manner that is targeted to specific muscle groups. This function could be particularly beneficial to subjects who have upper-extremity muscle imbalances, as the device could be set to provide resistance to the weak agonist muscle and not engage the stronger antagonist. More importantly, as we saw in our steering trials, SepaRRo could be used as a potential rehabilitation tool to engage normal muscle synergies (e.g., after stroke) by having subjects perform resisted reaching movements with steering angle directed in such a manner that it would engage the desired group of synergistic muscles (e.g., resisted reaching $0 \rightarrow 3$ with steering 45° to the left will target elbow extensors with shoulder abductors, which could target abnormal flexion synergy after stroke).

SepaRRo was created to fill the gap between fully assistive active robots and traditional passive exercise equipment. Although rehabilitation robots have tremendous upside for use in therapy (i.e., reduce manual effort by the therapist, standardize care, report outcomes, *etc.*), they are still being bypassed for less advanced passive devices because they fail to meet the logistical requirements to provide utility in clinic. Previous research indicates that ideal rehabilitation devices (including robots) should be designed in a manner to (1) encourage activities specific to daily living, (2) be able to be taken home, (3) have adjustable resistance to meet client needs, (4) have the potential to provide biofeedback to the clients, and (5) remain low-cost.[28] Typically, the cost of rehabilitation robots greatly exceeds what is recommended. We used controllable passive brakes on SepaRRo as a means to reduce the cost of the robot.

Currently, the manufacturing price for SepaRRo, including sensors, actuators, controller, manufacturing, *etc.*, is under $6,000USD (Supplementary Table 1) and we believe that the cost could substantially reduce with mass manufacturing. Although this is relatively affordable, the cost of such a device would have to increase if being sold commercially based on external economic factors (e.g., regulations, sales, distribution, *etc.*).

While this is still considerably more expensive then free weights or elastic bands, it is still far less expensive than active rehabilitation robots and the price is be comparable to professional weight training machines. Using these brakes had the additional benefit of increasing safety of the robot, which increases the likelihood that it can be taken home for rehabilitation. To further this point, the robot currently weighs just 12.1 kg, can be compacted to fit a $48 \times 40 \times 62$ cm^3 space, and can be mounted on any table (although this would sacrifice the ability to tilt the table). Hence, it could easily be transported and accommodate any rehabilitation space. Moreover, the large workspace and kinematic redundancies ensure that SepaRRo is able to target reaching movements while providing an adjustable resistive force-field with real-time biofeedback to the patient *via* the load-cell and encoders. These thoughts were confirmed by therapists who, after testing the robot, commented that the combination of resistance, large workspace, and steerability could "translate into real world activities, such as putting away groceries, washing dishes, *etc*." Further, they believed the steering and guidance could be useful to train coordination and accuracy in reaching tasks or to learn proper exercise techniques. However, the therapists did say that including different handles to accommodate patients with various grip and prehension abilities and incorporating a gaming interface to train functional tasks (e.g., reaching to grasp a cup) would be helpful.

Semi-passive devices such as SepaRRo are a substantial step toward bridging the disparity in functional capabilities between fully active robots and completely passive devices. Using motors, active robots provide a completely controllable (i.e., can assist, resist, and steer in any direction) interface for rehabilitation. However, this high level of functional capability is not required for patients who have residual abilities following an injury or are further along in their recovery. In this subpopulation, completely passive devices (e.g., elastic bands, weights, *etc*.) can be applied for therapy and obtained at a fraction of the cost. But these devices are greatly limited in their functional capabilities, as they can only provide linear resistances of fixed magnitudes and lack any controls, biofeedback, *etc*. SepaRRo is unique in that it is able to provide many of the functional capabilities of controllable active robots (resistance and steering), with many of the inherent accessibility benefits of passive devices. Hence, SepaRRo can be used to mimic many of the existing training modalities used for active robots, such as error reduction, where the user is encouraged to take a particular path that is programmed to be the path of least resistance; error augmentation, where the subject is provided with a perturbing steering force to push them off the desired path; or closed loop force/EMG based control, where the device can be set to require a certain level of effort from the subject.[30] These are all training modalities of semi-passive robots that would not be possible with completely passive devices. This middle ground of functional capability, combined with the logistical benefits mentioned above, make the semi-passive framework of SepaRRo an intriguing application of robotic therapy.

Limitations

There are some limitations to the work presented in this manuscript:

1. The robot was tested only on a small cohort of healthy subjects. This is reasonable given that we were only looking to provide proof of concept for how SepaRRo can be used to provide basic resistive forcefields.
2. We only present a single configuration of our SepaRRo prototype when there are many potential configurations (i.e., link lengths and the distance between the base of the two manipulators) that could drastically change the performance of the device. We chose the robot parameters based on our pilot simulations before designing the robot, but believe that these variables can be further optimized in order to change the shape of the workspace and to allow for better control (i.e., larger forces and steerable angles) within the regions where the subject will be using the device.
3. Our experiments were only performed across reaching paths that are commonly used during basic upper-extremity robotic rehabilitation (i.e., straightline reaching) due to experimental time constraints. As a result, the performance of the device was not experimentally evaluated across the entire workspace. However, since our experimental results were reasonably similar to the theoretical results on the tested workspace, we believe that the performance of the device can be extrapolated to the entire workspace using our theoretical plots.
4. Our controls currently do not account for the dynamics of the robot (e.g., inertia, friction, *etc*.), and this is a potential reason for why our desired and recorded forces had small errors during the hardware experiments. While we carefully designed the robot to minimize dynamics (e.g., locating the brakes as close to the base as possible *via* a timing belt), the effect of dynamics will increase as the angle of the table increases. For

example, as the table is tilted, gravity will act on the mass of the robots linkages. This would amplify the error between the desired and actual force felt at the end-effector. Thus, accounting for the dynamics of the robot in future iterations could reduce errors in the applied forces and steering angles.

Future Work

In addition to addressing many of the limitations noted above, there are numerous future studies to be performed, or improvements that can be made to the robot. The long-term goal of this research is for the robot to be used for rehabilitation in a clinical setting and eventually in the home. To meet this goal, we will have to show efficacy of the device by testing it in a clinical population (e.g., stroke). We may also need to fabricate a second, more rigid prototype using extruded aluminum tubing and high strength bearings, rather than the U-channels and small bearings used in this device. This more rigid prototype would be able to withstand the unintended forces seen with daily use (i.e., if a subject placed excess weight or leaned on the end-effector). Independent of these structural redesigns, we also plan to incorporate new control modalities in addition to the open-loop force magnitude and direction control demonstrated in this study. For example, we can incorporate closed loop control to render haptic objects, virtual walls, and paths within the workspace, or incorporate error augmentation to perturb the patient during training. Once these training modules are in place, we will need to revise the user interface to be simpler for a patient or therapist to operate and monitor progress. This can be accomplished by including pre-programmed training modalities, online data processing, and graphical tools to visualize progress. The interface could also be updated to include more game-like activities to better engage the patient in training.

Conclusion

In summary, this work presents a theoretical framework and offers a prototype to provide a proof of concept for SepaRRo, a semi-passive rehabilitation robot for functional resistance training of the upper-extremity. The results of this study indicate that, without active actuators or closed-loop controls, semi-passive robots can still provide an accurate and controllable interface for rehabilitation. Our findings unearth new possibilities for future rehabilitation robots based on semi-passive principles, as the technology can be further refined to provide unique forcefields to the user or extended for therapy of different patient populations. However, further testing is required to evaluate therapeutic potential in a patient population. So far, SepaRRo is a step towards our vision for rehabilitation robots that use semi-passive actuators so as to be cost-effective, lightweight, accessible in clinic or at home, and a potent tool for physical rehabilitation—potentially filling a large void in the current rehabilitation robotics landscape.

ELECTRONIC SUPPLEMENTARY MATERIAL

The online version of this article (https://doi.org/10.1007/s10439-018-2020-z) contains supplementary material, which is available to authorized users.

ACKNOWLEDGMENTS

Research reported in this publication was supported by (1) National Institute of Biomedical Imaging and Bioengineering (NIBIB) of the National Institutes of Health (Grant# R01-EB019834), (2) National Science Foundation Graduate Research Fellowship Program under Grant No. DGE #1256260, and (3) the University of Michigan Office of Research (UMOR) MCubed 2.0 program. The content is solely the responsibility of the authors and does not necessarily represent the official views of the funding agencies. A special thanks to Shannon Leon and Justin Lee for the work they did in building and programming the robot.

CONFLICT OF INTEREST

No benefits in any form have been or will be received from a commercial party related directly or indirectly to the subject of this manuscript.

REFERENCES

[1]Babaiasl, M., S. H. Mahdioun, P. Jaryani, and M. Yazdani. A review of technological and clinical aspects of robot-aided rehabilitation of upper-extremity after stroke. *Disabi. Rehabilit*. 11:263–280, 2016.

[2]Bertsekas, D. P. Nonlinear Programming, 2nd ed. Belmont: Athena Scientific, 1999.

[3]Bi, S., L. Ji, and Z. Wang. Robot-aided sensorimotor arm training methods based on neurological rehabilitation principles in stroke and brain injury patients. In: 27th Annual International Conference of the Engineering in Medicine and Biology Society, 2005. IEEE-EMBS 2005, pp. 5025–5027, 2006.

[4]BKin, R. N. M. Training with robot-applied resistance in people with motor-incomplete spinal cord injury: pilot study. *J. Rehabilit. Res. Dev*. 52:113, 2015.
[5]Book, W. J., R. Charles, H. T. Davis, and M. W. Gomes. The concept and implementation of a passive trajectory enhancing robot. Atlanta, GA: Georgia Institute of Technology, 1996.
[6]Brewer, B. R., R. Klatzky, and Y. Matsuoka. Initial therapeutic results of visual feedback manipulation in robotic rehabilitation. In: 2006 International Workshop on Virtual Rehabilitation, pp. 160–166, 2006.
[7]Chetran, B., D. Mândru, S. Noveanu, O. Tătar, and G. Răducanu. Electrorheological fluid based brake for active physiotherapy systems. *Acta Univ. Sapientiae Electr. Mech. Eng*. 4, 2012.
[8]Cho, C., M. Kim, and J.-B. Song. Performance analysis of a 2-link haptic device with electric brakes. Proceedings 11th Symposium on Haptic Interfaces for Virtual Environment and Teleoperator Systems, HAPTICS 2003, pp. 47–53, 2003.
[9]Cooper, R. A., B. E. Dicianno, B. Brewer, E. LoPresti, D. Ding, R. Simpson, G. Grindle, and H. Wang. A perspective on intelligent devices and environments in medical rehabilitation. *Med. Eng. Phys*. 30:1387–1398, 2008.
[10]Dellon, B. and Y. Matsuoka. Path guidance control for a safer large scale dissipative haptic display. In: IEEE International Conference on Robotics and Automation, 2008. ICRA 2008, pp. 2073–2078, 2008.
[11]Dewald, J. P., P. S. Pope, J. D. Given, T. S. Buchanan, and W. Z. Rymer. Abnormal muscle coactivation patterns during isometric torque generation at the elbow and shoulder in hemiparetic subjects. *Brain* 118:495–510, 1995.
[12]Duschau-Wicke, A., A. Caprez, and R. Riener. Patient-cooperative control increases active participation of individuals with sci during robot-aided gait training. *J. Neuroeng. Rehabilit*. 7:43, 2010.
[13]Daz, I., J. J. Gil, and E. Snchez. Lower-limb robotic rehabilitation: literature review and challenges. *J. Robot*. https://doi.org/10.1155/2011/759764, 2011.
[14]Fukushi, T. and J. Ashe. Adaptation of arm trajectory during continuous drawing movements in different dynamic environments. *Exp. Brain Res*. 148:95–104, 2003.
[15]Gao, D. Control limitation analysis for dissipative passive haptic interfaces. Ph.D. thesis, Georgia Institute of Technology, 2005.
[16]Gao, D. and W. J. Book. Steerability for planar dissipative passive haptic interfaces. *IEEE/ASME Transa. Mech*. 11:179–184, 2006.
[17]Gao, D. and W. J. Book. Steerability in planar dissipative passive robots. *Int. J. Robot. Res*. 29:353–366, 2010.
[18]Genduso, F., R. Miceli, C. Rando, and G. R. Galluzzo. Back emf sensorless-control algorithm for high-dynamic performance pmsm. *IEEE Trans. Ind. Electron*. 57:2092–2100, 2010.
[19]Haraguchi, M. and J. Furusho. Passive-type rehabilitation system for upper limbs which can display the exact resistance force in the orientation opposite to hand motion. In: 2013 IEEE International Conference on Rehabilitation Robotics (ICORR), pp. 1–6, 2013.
[20]Hesse, S., H. Schmidt, C. Werner, and A. Bardeleben. Upper and lower extremity robotic devices for rehabilitation and for studying motor control. *Curr. Opin. Neurol*. 16:705–710, 2003.
[21]Hesse, S., G. Schulte-Tigges, M. Konrad, A. Bardeleben, and C. Werner. Robot-assisted arm trainer for the passive and active practice of bilateral forearm and wrist movements in hemiparetic subjects. *Arch. Phys. Med. Rehabilit*. 84:915–920, 2003.
[22]Johnson, M. J., X. Feng, L. M. Johnson, and J. M. Winters. Potential of a suite of robot/computer-assisted motivating systems for personalized, home-based, stroke rehabilitation. *J. Neuro Eng. Rehabilit*. 4:6, 2007.
[23]Khatib, O., V. Kumar, and G. Sukhatme. Experimental Robotics: The 12th International Symposium on Experimental Robotics, Vol. 79. New York: Springer, 2013.
[24]Kikuchi, T., H. Xinghao, K. Fukushima, K. Oda, J. Furusho, and A. Inoue. Quasi-3-dof rehabilitation system for upper limbs: its force-feedback mechanism and software for rehabilitation. In: IEEE 10th International Conference on Rehabilitation RoboFtics, 2007. ICORR 2007, pp. 24–27, 2007.
[25]Krishnan, C., K. Huston, A. Amendola, and G. N. Williams. Quadriceps and hamstrings muscle control in athletic males and females. *J. Orthop. Res*. 26:800–808, 2008.
[26]Krishnan, C., R. Ranganathan, Y. Y. Dhaher, and W. Z. Rymer. A pilot study on the feasibility of robot-aided leg motor training to facilitate active participation. *PloS ONE* 8:e77370, 2013.
[27]Lawson, C. L. and R. J. Hanson. Solving least squares problems. In: Classics in Applied Mathematics. Philadelphia: Society for Industrial and Applied Mathematics, pp. 158–173, 1995.
[28]Lu, E. C., R. H. Wang, D. Hebert, J. Boger, M. P. Galea, and A. Mihailidis. The development of an upper limb stroke rehabilitation robot: identification of clinical practices and design requirements through a survey of therapists. *Disabil. Rehabilit*. 6:420–431, 2011.
[29]Maciejasz, P., J. Eschweiler, K. Gerlach-Hahn, A. Jansen-Troy, and S. Leonhardt. A survey on robotic devices for upper-limb rehabilitation. *J. Neuro Eng. Rehabilit*. 11:3, 2014.
[30]Marchal-Crespo, L. and D. J. Reinkensmeyer. Review of control strategies for robotic movement training after neurologic injury. *J. Neuro Eng. Rehabilit*. 6:20, 2009.
[31]Mares, K., J. Cross, A. Clark, G. R. Barton, F. Poland, M. L. O'Driscoll, M. J. Watson, K. Mcglashan, P. K. Myint, and V. M. Pomeroy. The FeSTivaLS trial protocol: a randomized evaluation of the efficacy of functional strength training on enhancing walking and upper limb function later post stroke. *Int. J. Stroke* 8:374–382, 2013.
[32]Munir, S., L. Tognetti, and W. Book. Experimental evaluation of a new braking system for use in passive haptic displays. In: American Control Conference, 1999. Proceedings of the 1999, Vol. 6, pp. 4456–4460, 1999.
[33]Pollock, A., G. Baer, P. Campbell, P. L. Choo, A. Forster, J. Morris, V. M. Pomeroy, and P. Langhorne. Physical rehabilitation approaches for the recovery of function and mobility following stroke. *Cochrane Database Syst. Rev*. 4:CD001920, 2014.
[34]Qian, Z. and Z. Bi. Recent development of rehabilitation robots. *Adv. Mech. Eng*. 7:563062, 2015.
[35]Reed, M. R. and W. J. Book. Modeling and control of an improved dissipative passive haptic display. In: 2004 IEEE International Conference on Robotics and Automation, 2004. Proceedings ICRA'04, Vol. 1, pp. 311–318, 2004.
[36]Reinkensmeyer, D. J., J. L. Emken, and S. C. Cramer. Robotics, motor learning, and neurologic recovery. *Annu. Rev. Biomed. Eng*. 6:497–525, 2004.
[37]Schwartz, I. and Z. Meiner. Robotic-assisted gait training in neurological patients: who may benefit? *Ann. Biomed. Eng*. 43:1260–1269, 2015.

[38]Senkal, D. and H. Gurocak. Haptic joystick with hybrid actuator using air muscles and spherical mr-brake. *Mechatronics* 21:951–960, 2011.
[39]Stienen, A. H., E. E. Hekman, F. C. Van der Helm, G. B. Prange, M. J. Jannink, A. M. Aalsma, and H. Van der Kooij. Dampace: dynamic force-coordination trainer for the upper extremities. In: IEEE 10th International Conference on Rehabilitation Robotics, 2007. ICORR 2007, pp. 820–826, 2007.
[40]Thanh, T. D. C. and K. K. Ahn. Intelligent phase plane switching control of pneumatic artificial muscle manipulators with magneto-rheological brake. *Mechatronics* 16:85–95, 2006.
[41]Vasavada, A. N., B. W. Peterson, and S. L. Delp. Three-dimensional spatial tuning of neck muscle activation in humans. *Exp. Brain Res.* 147:437–448, 2002.
[42]Washabaugh, E. P., E. S. Claflin, R. B. Gillespie, and C. Krishnan. A novel application of Eddy current braking for functional strength training during gait. *Ann. Biomed. Eng.* 44:2760–2773, 2016.
[43]Weightman, A., A. Alexoulis-Chrysovergis, and S. Oltean. What should we consider when designing rehabilitation robots for the upper limb of the neurologically impaired? Proceedings of the Australasian Conference on Robotics and Automation pp. 1–10, 2014.
[44]Weightman, A., N. Preston, M. Levesley, R. Holt, M. Mon-Williams, M. Clarke, A. J. Cozens, and B. Bhakta. Home-based computer-assisted upper limb exercise for young children with cerebral palsy: a feasibility study investigating impact on motor control and functional outcome. J. Rehabilit. Med. 43:359–363, 2011.
[45]Williams, G. N., P. J. Barrance, L. Snyder-Mackler, M. J. Axe, and T. S. Buchanan. Specificity of muscle action after anterior cruciate ligament injury. *J. Orthop. Res.* 21:1131–1137, 2003.
[46]Willmann, R. D., G. Lanfermann, P. Saini, A. Timmermans, J. te Vrugt, and S. Winter. Home stroke rehabilitation for the upper limbs. In: 29th Annual International Conference of the IEEE Engineering in Medicine and Biology Society, pp. 4015–4018, 2007.
[47]Yang, Y.-R., R.-Y. Wang, K.-H. Lin, M.-Y. Chu, and R.-C. Chan. Task-oriented progressive resistance strength training improves muscle strength and functional performance in individuals with stroke. *Clin. Rehabilit.* 20:860–870, 2006.

Annals of Biomedical Engineering, Vol. 46, No. 11, November 2018 *(© 2018)* p. 1962
https://doi.org/10.1007/s10439-018-2096-5

Correction

Correction to: A Semi-passive Planar Manipulandum for Upper-Extremity Rehabilitation

Chih-Kang Chang,[1] Edward P. Washabaugh,[1,2] Andrew Gwozdziowski,[1] C. David Remy,[3,4] and Chandramouli Krishnan[1,2,4]

[1]Neuromuscular and Rehabilitation Robotics Laboratory (NeuRRo Lab), Department of Physical Medicine and Rehabilitation, University of Michigan, Ann Arbor, MI, USA; [2]Department of Biomedical Engineering, University of Michigan, Ann Arbor, MI, USA; [3]RAM Lab, Department of Mechanical Engineering, University of Michigan, Ann Arbor, MI, USA; and [4]Michigan Robotics, College of Engineering, University of Michigan, Ann Arbor, MI, USA

Correction to:
Annals of Biomedical Engineering,
Vol. 46, No. 7, July 2018, pp. 1047–1065
https://doi.org/10.1007/s10439-018-2020-z

Authors would like to correct their acknowledgments. Correct acknowledgments appear here.

ACKNOWLEDGMENTS

Research reported in this publication was supported by (1) Disability and Rehabilitation Engineering (DARE) Program of the National Science Foundation (Award# 1804053), (2) National Institute of Biomedical Imaging and Bioengineering (NIBIB) of the National Institutes of Health (Grant# R01 EB019834), (3) National Science Foundation Graduate Research Fellowship Program under Grant No. DGE #1256260, and (4) the University of Michigan Office of Research (UMOR) MCubed 2.0 program. The content is solely the responsibility of the authors and does not necessarily represent the official views of the funding agencies. A special thanks to Shannon Leon and Justin Lee for the work they did in building and programming the robot.

Address correspondence to Chandramouli Krishnan, Neuromuscular and Rehabilitation Robotics Laboratory (NeuRRo Lab), Department of Physical Medicine and Rehabilitation, University of Michigan, Ann Arbor, MI, USA. Electronic mail: mouli@umich.edu

The original article can be found online at https://doi.org/10.1007/s10439-018-2020-z.

0090-6964/18/1100-1962/0 © 2018 Biomedical Engineering Society